# Improving resilience of quantum-gravity-induced entanglement of masses to decoherence using three superpositions

Martine Schut, 1,2,\* Jules Tilly, 3,† Ryan J. Marshman, Sougato Bose, 3,8 and Anupam Mazumdar, Wan Swinderen Institute for Particle Physics and Gravity, University of Groningen, 9747 AG Groningen, Netherlands

Bernoulli Institute for Mathematics, Computer Science and Artificial Intelligence, University of Groningen, 9747 AG Groningen, Netherlands

Department of Physics and Astronomy, University College London, Gower Street, WC1E 6BT London, United Kingdom

(Received 16 November 2021; accepted 3 February 2022; published 4 March 2022)

Recently, a protocol called quantum-gravity-induced entanglement of masses (QGEM) that aims to test the quantum nature of gravity using the entanglement of two qubits was proposed. The entanglement can arise only if the force between the two spatially superposed masses is occurring via the exchange of a mediating virtual graviton. In this paper we examine a possible improvement of the QGEM setup by introducing a third mass with an embedded qubit so that there are now three qubits to witness the gravitationally generated entanglement. We compare the entanglement generation for different experimental setups with two and three qubits and find that a three-qubit setup where the superpositions are parallel to each other leads to the highest rate of entanglement generation within  $\tau = 5$  s. We show that the three-qubit setup is more resilient to the higher rate of decoherence. The entanglement can be detected experimentally for the two-qubit setup if the decoherence rate  $\gamma$  is  $\gamma < 0.11$  Hz compared to  $\gamma < 0.16$  Hz for the three-qubit setup. However, the introduction of an extra qubit means that more measurements are required to characterize entanglement in an experiment. We conduct experimental simulations and estimate that the three-qubit setup would allow detecting the entanglement in the QGEM protocol at a 99.9% certainty with  $O(10^4)$ – $O(10^5)$  measurements when  $\gamma \in [0.1, 0.15]$  Hz. Furthermore, we find that the number of needed measurements can be reduced to  $O(10^3)$ – $O(10^5)$  if the measurement schedule is optimized using joint Pauli basis measurements. For  $\gamma > 0.06$  Hz the three-qubit setup is favorable compared to the two-qubit setup in terms of the minimum number of measurements needed to characterize the entanglement. Thus, the proposed setup here provides a promising avenue for implementing the QGEM experiment.

DOI: 10.1103/PhysRevA.105.032411

#### I. INTRODUCTION

The quantum or classical nature of gravity has long been a central theme in theoretical physics [1]. Unlike other interactions of nature, gravity remains the only known interaction whose quantum behavior has never been observed in a laboratory. It is believed that the spin-2 massless graviton is the carrier of gravitational interaction, which can be canonically quantized around a Minkowski background [2–5]. However, the direct detection of a graviton remains extremely difficult due to the weakness of the gravitational interaction compared to the other fundamental interactions of nature [6,7]. Even the direct detection of primordial gravitational waves will not be able to falsify the quantum nature of graviton [8,9]. The indirect detection of the quantum aspects of graviton may be feasible in the near future in laboratory-based experiments.

Recently, there has been a proposal to witness the quantum nature of gravity by witnessing the entanglement of masses [10], with the theoretical protocol outlined in [10,11]. Simultaneously, there was another paper [12] where the authors proposed to witness the quantum nature of gravity by witnessing entanglement. However, the detailed analysis of the graviton as a mediator and the feasibility aspects of the experiment including decoherence and the relevant background were first discussed in Ref. [10]. The proposal was followed by extensive interest in the research community, suggesting extensions and variations [13–34]. The protocol is based on a bona fide quantum-mechanical gravitational interaction which cannot be replicated by a classical world. One of the main experimental requirements is the creation of the spatial quantum superposition of masses, i.e., creating Schrödinger cat states, in a laboratory. For the detection of quantum aspects of gravity, we require the generation of quantum entanglement, which yields quantum correlations between any two quantum states and has no classical analog [35]. We assume that no other quantum interactions arise between the systems. To prove that the detection of entanglement shows the quantum nature of gravity, we rely on the properties of the local operations and classical communication (LOCC) principle [36,37]. The LOCC principle states that the two quantum states cannot be entangled via a classical channel if they were not entangled to begin with, or entanglement cannot be increased by local operations and classical communication. The classical communication is the critical ingredient which can be put to test

<sup>\*</sup>martine.schut@rug.nl

<sup>†</sup>jules.tilly.18@ucl.ac.uk

<sup>‡</sup>r.marshman@uq.edu.au

<sup>§</sup>s.bose@ucl.ac.uk

<sup>&</sup>lt;sup>∥</sup>anupam.mazumdar@rug.nl

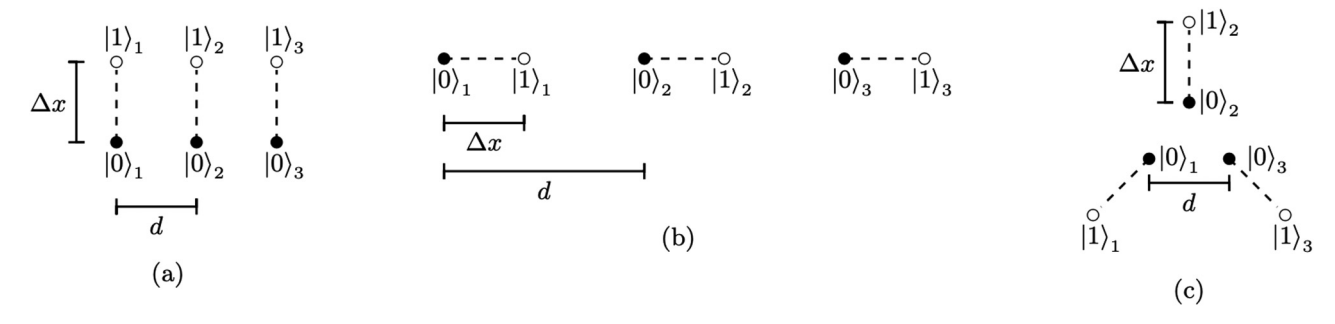


FIG. 1. Proposed setups of the QGEM experiment using three qubits in spatial superpositions aligned in different configurations. The superposition states of the *i*th qubit are denoted by  $|0\rangle_i$  and  $|1\rangle_i$ . The minimal distance  $d_{\min} = 200~\mu m$  between any two states and the superposition width  $\Delta x = 250~\mu m$  [10] is kept constant in all different setups. The distance d denotes the distance between any two neighboring  $|0\rangle$  states and is determined by the setup. (a) Parallel setup of the three-qubit QGEM experiment where the spatial superpositions are aligned parallel to each other. Note that  $d_{\min} = d < \Delta x$ . (b) Linear setup of the three-qubit QGEM experiment where the spatial superpositions are aligned linearly to each other. Note that  $d = d_{\min} + \Delta x > \Delta x$ . (c) Star setup of the three-qubit QGEM experiment where the spatial superpositions are aligned in a manner we label as a star pattern. Note that  $d_{\min} = d < \Delta x$ .

when it comes to graviton-mediated interaction between the two masses. If the graviton is quantum, it could mediate the gravitational attraction between the two masses and it would also entangle them, hence giving rise to the quantum-gravityinduced entanglement of masses (QGEM) proposal [10,11]. The OGEM protocol highlighted the requirement of a graviton as a quantum mediator, implying the origin of the gravitational force between masses can be viewed as resulting from the exchange of a virtual graviton. A virtual graviton is not a classical entity and does not satisfy the classical equations of motion; there is a total of six off-shell degrees of freedom, i.e., spin-2 and spin-0 components, in the graviton propagator (see [11,38,39]). By witnessing the entanglement between the two masses and by detecting a correlation between the spins which are embedded in the two test masses, we can ascertain whether the exchange of the virtual graviton is a classical or a quantum entity [10,11].

Many possible improvements to the original setup have already been discussed, using a different witness [19], ways of creating macroscopic quantum superposition [16], including effects due to decoherence [19,40], ameliorating Casimirinduced entanglement [17], taming gravity gradient noise and relative acceleration [18,20], a different configuration of the superpositions [14], using higher-dimensional quantum objects [24], or using different measurement bases [41]. Furthermore, Refs. [21,22] propose that the QGEM experiment may be used to gain insights into the Planck mass and the discreteness of time and possibly probe nonlocal gravitational interaction [11,42,43]. The nonlocal gravitational interaction tends to weaken the entanglement witness and the entanglement entropy [11].

In this paper we will explore a design with three masses, each with an embedded qubit (instead of two masses with two qubits as proposed in the original QGEM protocol [10]). As we will witness the entanglement purely by measuring the qubits, we will refer to the previous and our current protocols henceforth as two-qubit and three-qubit protocols, respectively. We will show that this three-qubit protocol performs better at generating entanglement, in particular when the decoherence effects are taken into account. However, this comes at the cost of requiring more measurements to characterize

entanglement with a good enough level of certainty. In Sec. II different possible setups for a three-qubit QGEM experiment will be discussed. The optimal setup will be identified by comparing the rate of entanglement generation in Sec. III. In Sec. IV we will discuss the witness expectation value for the different setups. In Sec. V we will incorporate the decoherence in our analysis, to test how robust the different setups are to different decoherence rates. Section VI will discuss experimental simulations and the number of measurements needed to characterize the entanglement. We will consider possible improvements by switching to qudits instead of qubits and discuss the merits of this approach in Sec. VII.

A short summary of our paper is that we find that the three-qubit parallel setup [see Fig. 1(a)] is better than other configurations with three qubits including the decoherence effects taken into account. Moreover, the entanglement entropy is dependent on the chosen subsystem. Taking the partial trace of the *middle* qubit gives the largest entanglement entropy. Similarly, when determining the witness, choosing the middle qubit as the subsystem provides an improved witness. The three-qubit setup outperforms the two-qubit setup in generating entropy within 5 s and it has a better witness. Furthermore, entanglement can be measured up to higher decoherence rates, and the number of measurements needed to confirm entanglement at higher decoherence rates  $\gamma > 0.08$  Hz is similar to or smaller than for the two-qubit setup.

# II. THREE-QUBIT QGEM SETUP

We first discuss the optimal setups for the two- and threequbit cases. Reference [14] found that for the two-qubit setup it is favorable to create the superpositions in the direction orthogonal to their separation [depicted in Fig. 1(a)], as opposed to in the same direction as their separation, which was

<sup>&</sup>lt;sup>1</sup>Throughout this paper the number of superpositions is denoted by n and the number of states in the superposition is denoted by D. For spin systems, the value of D = 2s + 1, where s is the spin state, for electronic spin  $s = \frac{1}{2}$ . Later we will consider qudits which have D superposition states, but for now we consider only qubits (D = 2)

proposed in the original paper [10] [depicted in Fig. 1(b)]. We will first introduce three different setups [Figs. 1(a)–1(c)] and in the next section we will study the generation of the entanglement in each setup to determine the better configuration for witnessing graviton-induced entanglement.

For any three-qubit setup the initial (unentangled) state is given as<sup>2</sup>

$$|\Psi_0\rangle = \frac{1}{2\sqrt{2}} \bigotimes_{i=1}^3 (|0\rangle_i + |1\rangle_i). \tag{1}$$

The gravitational interaction between the two states is governed by the universal coupling  $\sqrt{G}h_{\mu\nu}T^{\mu\nu}$ , where the metric is  $g_{\mu\nu} = \eta_{\mu\nu} + h_{\mu\nu}$ , with  $\mu, \nu = 0, 1, 2, 3$ , and  $h_{\mu\nu}$  is the perturbation around the Minkowski background  $\eta_{\mu\nu}$ . Due to the gravitational interaction, each superposition state picks up a relative quantum-mechanical phase  $\phi \sim S/\hbar \sim \frac{E\tau}{\hbar}$ , where S is the gravitational action. This can be viewed as the result of the time-evolution operator or equivalently as a result of the Feynman path-integral formalism for a particle moving through spacetime. The interaction energy E is determined by the gravitational potential energy V, which in the nonrelativistic case is derived from the tree-level exchange of a virtual graviton [11]. The quantum origin of this potential in the nonrelativistic limit of perturbative quantum gravity in the weak-field regime is discussed in detail in Refs. [11,44]. The effect of higher-order corrections will be negligible here.

The total gravitational potential energy is given by  $\hat{V}_{\text{tot}} = \hat{V}_{12} + \hat{V}_{23} + \hat{V}_{13}$ , where the subscripts denote the interactions between the subsystems. For example,  $\hat{V}_{ij}$  is the potential energy between system i at  $x_i$  and system j at  $x_j$ , which is given by  $\frac{Gm_im_j}{|\hat{x}_i-\hat{x}_j|}$ .

We now give the system's state after the qubits have gravitationally interacted. To avoid writing out all the terms, we will use the shorthand notation where  $j_i = 0, 1$  denotes the state of the *i*th qubit (so  $|j_i\rangle$  is either  $|0\rangle$  or  $|1\rangle$ ),

$$|\Psi(t=\tau)\rangle = \frac{1}{2\sqrt{2}} \sum_{j_1, j_2, j_3=0.1} e^{i\phi_{j_1 j_2 j_3} \tau} |j_1 j_2 j_3\rangle,$$
 (2)

with  $\phi_{j_1j_2j_3}\tau$  the phase picked up due to the interaction via gravity between the systems during a time  $\tau$  for the state  $|j_1j_2j_3\rangle$ . Note that since  $\phi_{j_1j_2j_3}$  is simply  $U_{\text{tot}}/\hbar$ , it is determined by the distance between the states  $|x_i-x_j|$ . Since the setup specifies the distance between two systems, the phases are specific to the setup. For the parallel setup in Fig. 1(a) we find

$$\phi_{j_1 j_2 j_3}^{(\parallel)} = \frac{1}{\hbar} \sum_{i,k=1,2,3}^{i < k} \frac{Gm^2}{\sqrt{d^2 + [\Delta x (j_i - j_k)]^2}}.$$
 (3)

The superscript  $\parallel$  specifies the parallel setup. For the linear setup in Fig. 1(b) (denoted by -) we find

$$\phi_{j_1 j_2 j_3}^{(-)} = \frac{1}{\hbar} \sum_{i,k=1,2,3}^{i < k} \frac{Gm^2}{(k-i)d + \Delta x(j_k - j_i)}$$
(4)

and for the star setup (denoted by \*) we find

$$\phi_{j_1 j_2 j_3}^{(*)} = \frac{1}{\hbar} \sum_{i,k=1,2,3}^{i < k} \frac{Gm^2}{r_{ik}},\tag{5}$$

where  $r_{ik}$  is the distance between the superposition instances labeled i and k in the star setup:

$$r_{ik} = (1 - j_i j_k)d + j_i j_k (d + \sqrt{\Delta x}) + (j_k - j_i)(\sqrt{d^2 + \sqrt{3}d\Delta x + \Delta x^2} - d).$$
 (6)

The expressions for the distances were found using trigonometry. The distance d between two neighboring  $|0\rangle$  states is determined by the superposition width  $\Delta x = 250~\mu m$  and by requiring a minimal distance between any two qubits  $d_{\rm min} = 200~\mu m$ . This minimum distance is introduced to ensure that the Casimir-Polder potential is negligible [10]. Due to the chosen parameters, the separation between the two qubits in the parallel setup is  $d = 200~\mu m$ , for the linear setup it is  $d = 450~\mu m$ , and for the star setup the edge of the inner triangle is  $d = 200~\mu m$ . Furthermore, we will consider the masses of  $m \sim 10^{-14}~kg$  and an interaction time of  $\tau_{\rm int} = 2.5~s$ . These parameters fall within the feasible range discussed in [10,16].

From Eq. (2) we find that the density matrix of the system is  $\rho(\tau) = |\Psi(\tau)\rangle\langle\Psi(\tau)|$ ,

$$\rho(\tau) = \frac{1}{8} \sum_{\substack{j_1, j_2, j_3 = 0, 1 \\ j'_1, j'_2, j'_3 = 0, 1}} e^{i(\phi_{j_1, j_2, j_3} - \phi_{j'_1, j'_2, j'_3})\tau} \bigotimes_{i, i' = 1, 2, 3} |j_i\rangle\langle j'_{i'}|. \tag{7}$$

For more on the density matrix formalism, see [45]. With Eq. (7), we can analyze and compare the rate of entanglement generation for the different setups, which we will do by studying the entanglement entropy.

## III. ENTANGLEMENT ENTROPY TEST

As an initial test for comparing the two-qubit setup with the three-qubit setup, we assess the rate of entanglement generation for each version of the experiment. To do so, we will rely

<sup>&</sup>lt;sup>2</sup>Note that the different denotations for the three-qubit state used in this paper refer to equivalent states, that is,  $\bigotimes_{i=1}^{3} |0\rangle_{i} = |0\rangle_{1} \otimes |0\rangle_{2} \otimes |0\rangle_{3} = |0_{1}0_{2}0_{3}\rangle$ . The state of the *i*th qubits is generally denoted by  $j_{i} = 0, 1$ . For compactness and clarity, different denotation is used throughout this paper.

<sup>&</sup>lt;sup>3</sup>The considered setups of Fig. 1 are symmetrical in d (and m). Considering asymmetric configurations where one of the distances is increased above  $d_{\min}$  is not favorable since it decreases the interaction which goes as 1/r. (Similarly considering asymmetric configurations where one of the masses is smaller than what is considered the largest possible mass m is not favorable since it decreases the interaction strength.)

 $<sup>^4</sup>$ The interaction time of  $\tau_{int}=2.5$  s was chosen because it is both feasible experimentally and during this time the systems can become entangled enough to be detectable [11,23]. If the interaction time were decreased, we will see in Figs. 2, 6, and 7 that the three-qubit setup still generates more entanglement and provides a better witness.

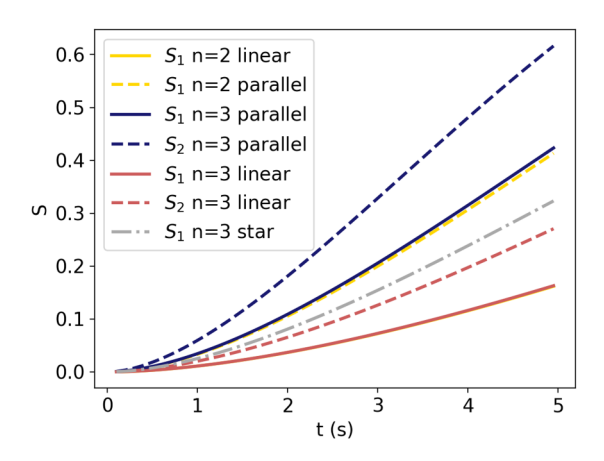


FIG. 2. Comparison of the entanglement entropy generated within 5 s. Note that, due to the symmetry of the setups, for the parallel and linear setups we have  $S_1 = S_3$  and for the star setup we have  $S_1 = S_2 = S_3$ . During the first 5 s the n = 3 parallel setup has the highest rate of entanglement generation compared to the other setups. The lines representing  $S_1$ , n = 3 linear and  $S_1$ , n = 2 linear setups almost overlap. The same plot for a larger timescale is given in Fig. 15 in Appendix C.

on the entanglement entropy (von Neumann entropy) which measures the overall mixing of one of the subsystems of the two- or three-particle quantum state.

Using the density-matrix formalism, the entanglement entropy can be found as [46,47]

$$S(\rho_a) = -\text{Tr}[\rho_a \log_2(\rho_a)] = -\sum_i \lambda_i \log_2(\lambda_i), \quad (8)$$

where  $\rho_a$  is the partial density matrix of the subsystems a with the eigenvalues  $\lambda_i$ . The partial density matrix of a subsystem is found by taking the partial trace over the other subsystems, e.g., the partial density matrix describing the first system is defined by  $\rho_1 = \text{Tr}_{2,3}(\rho)$  and can be used to find the entanglement entropy of the first subsystem  $S_1$ . Here  $\text{Tr}_{2,3}$  denotes the partial trace over subsystems 2 and 3. Although the entanglement entropy will be identical for either subsystem in the two-qubit case ( $S_1 = S_2$ ), this is not the case when adding a third qubit, as we now have several options for the system's partition.

We compare the entanglement entropy for the three-qubit system with the two-qubit system and find that an improvement is made for the parallel setup, especially for  $S_2$ , as can be seen from Fig. 2. For the two-qubit setup (n = 2) we have considered the linear and parallel setups, which were discussed previously in [10,14], respectively. Their state and density matrix can be derived from Eq. (7) by leaving out the third particle  $j_3$ . We have compared the two-qubit (n = 2) setups with the three-qubit (n = 3) parallel, linear, and star setups [depicted in Figs. 1(a)-1(c), respectively].

From Fig. 2 it is clear that the setup that generates the most entropy is the parallel three-qubit  $S_2$ . This setup considers the entropy between the middle subsystem (labeled 2) and the outer subsystems (labeled 1 and 3). As noted above,  $S_2 > S_1 = S_3$ , meaning the entanglement entropy is dependent on which systems are chosen to be traced out. A likely explanation for these differences is that the average distance

to the other subsystems is smaller for system 2 than for system 1 or 3 [see Fig. 1(a)] and therefore it has a higher coupling to the other subsystems. Note that, due to the symmetries of the setup, for the linear and parallel cases we have  $S_1 = S_3$  and for the star setup we have  $S_1 = S_2 = S_3$ . From now on, when considering the parallel or linear n = 3 setup we will always consider the second subsystem  $S_2$  (unless specified otherwise).

Of course, the use of entanglement entropy as a figure of merit for an experimental setup is not fully reliable. The introduction of noise in the experiment and overall a realistic setting make it impossible to distinguish the mixed state from entanglement and the mixing resulting from the decoherence of the states. As such, following previous research on this experiment [10,14,19,24], we compare the different systems in terms of the possibility of identifying the entanglement in a realistic setting by using the entanglement witness.

## IV. ENTANGLEMENT WITNESS

For the experimental detection of the entanglement one needs a witness, as discussed in [10]. The witness will be derived from a condition that determines when the states are separable or entangled. In Ref. [10], the witness was derived from the witness for the Bell state. These types of witnesses are often not ideal in an experimental setup [48].

Reference [19] proposed a new witness based on the positive partial trace (PPT) criterion for separability of mixed states [49,50]. In the two-qubit case, this witness was found to work up to higher decoherence rates when decoherence was introduced into the model [19]. In [24], which considered the two-particle QGEM with qudits, the PPT witness was also found to be an optimal witness and more efficient at detecting the entanglement than alternatives. For the three-qubit setup explored in this paper, we will therefore also use the PPT witness.

The PPT witness gives the following criterion for the separability of the states: A state  $\rho$  is separable if and only if its partial transpose is positive semidefinite, which is analogous to having no negative eigenvalues [51]. The partial transpose of the density matrix in Eq. (7) is found to be

$$\rho^{T_2}(\tau) = \frac{1}{8} \sum_{\substack{j_1, j_2, j_3 = 0, 1\\ j'_1, j'_2, j'_3 = 0, 1}} e^{i(\phi_{j_1 j'_2 j_3} - \phi_{j'_1 j_2 j'_3})\tau} \bigotimes_{i, i' = 1, 2, 3} |j_i\rangle\langle j'_{i'}|, \quad (9)$$

where the superscript  $T_2$  denotes the partial transpose of the second system is taken (similarly to  $S_2$ , transposing the middle subsystem provides a better witness because of the chosen partition). Note that since the phase  $\phi = \phi^{(\parallel)}, \phi^{(-)}, \phi^{(*)}$  differs for the different setups in Fig. 1, the witness will also be different for each of the three setups. According to the PPT criterion, the system is entangled if the PPT density matrix (9) has negative eigenvalues.

We will use this criterion to construct the entanglement witness W, which is an observable that provides a sufficient (but not always necessary) condition to detect entanglement. We construct the witness [49]

$$W = |\lambda_{-}\rangle\langle\lambda_{-}|^{T}, \tag{10}$$

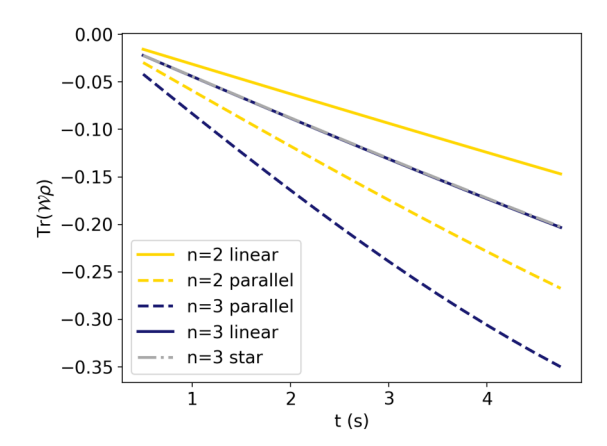


FIG. 3. Expectation value of the PPT witness W with respect to time. For the three-qubit cases we have considered  $\rho^{T_2}$ , meaning that system 2 is transposed as in Eq. (9). The lines representing the n=3 linear and star setups approximately overlap. We see that in the chosen basis the n=3 parallel setup provides the best (most negative) witness.

where  $|\lambda_{-}\rangle$  is the eigenvector corresponding to the smallest eigenvalue of  $\rho^{T}$  (the partial transpose of  $\rho$ ). All separable states  $\rho$  then satisfy [49]

$$\operatorname{Tr} \mathcal{W} \rho \geqslant 0.$$
 (11)

If  ${\rm Tr}{\cal W}\rho<0$ , the state  $\rho$  has negative eigenvalues and is therefore an entangled state. Note that for the three-qubit case, the witness is a sufficient but not necessary condition for the entanglement generation, meaning that if  ${\rm Tr}\rho{\cal W}\geqslant 0$ , the state can be either separable (not entangled) or nonseparable (entangled). An example of such a three-qubit entangled state with  ${\rm Tr}\rho{\cal W}\geqslant 0$  is given in [52]. The exact expressions for the witness operators for the two- and three-qubit setups are given in Appendix A in terms of Pauli observables.

The expectation values of the PPT entanglement witness for the setups discussed in Sec. II are shown in Fig. 3. The three-qubit parallel setup does very well compared to the other setups, which makes us optimistic about its potential for detecting the entanglement. Since the witness is basis dependent, one can only compare the shapes and should be careful in comparing the values. Nevertheless, Fig. 3 shows a much faster decrease in the entanglement witness expectation value for the parallel three-qubit setup compared to the other setups.

Although adding a qubit seems to yield a better witness, it also comes with a more difficult experimental setup. We can decompose the witness in terms of Pauli matrices, which can be measured experimentally. Examples of these decompositions for two and three qubits are shown in Appendix A.

In general, given each particle can be measured in one of three Pauli basis elements (plus identity), there is a total of  $O(4^n)$  terms to be measured for an entanglement witness acting on n particles. The number of Pauli matrices that need to be measured scales exponentially with the number of qubits, therefore increasing exponentially the number of measurements required to characterize the entanglement.

Given that we aim to produce the experimental setup that is most efficient in detecting the entanglement, this could become a large impediment to using three or more qubits. As an illustration, while the two-qubit setup requires the measurement of only three operators to construct the witness, the three-qubit setup requires 25 operators to be measured.

To address this issue, we will turn towards the literature regarding grouping a list of Pauli matrices into Abelian (commutative) groups, traditionally used in quantum computing (and initially stemming from error correction theory). Pauli matrices that commute with each other can be jointly diagonalized by basis rotation [53], allowing them to be jointly measured. Grouping of terms for the QGEM experiment with qudits was proposed in [24] by identifying groups based on general commutativity of the operators [54-56]. However, authors noted that the realization of the joint measurements by following this type of grouping may require nonlocal operations.<sup>5</sup> These techniques are widely used in the context of early-stage quantum computation to reduce the number of measurements required to perform methods such as the variational quantum eigensolver (see [59]). Here we propose to group Pauli matrices based on qubitwise commutation [57,60–64] rather than the general commutation (i.e., we group two Pauli matrices together if each qubit operator commutes in the first matrix commutes with the respective qubit operator in the second matrix) [54–57]. While this in general means that fewer savings can be achieved in terms of the total number of measurements we can perform, these joint measurements can be realized through local operations only. It is worth noting as well that such grouping strategies could result in additional sampling noise from the appearance of covariance between the operators being measured jointly [60]. These were shown however to be the exception rather than the rule [57], and therefore we will leave the detailed analysis of these possible covariances to future analyses. To perform the grouping, we use the largest-degree-first coloring (LDFC) algorithm [65], though for a small number of particles this can be done manually. The LDFC algorithm is a traditional heuristic algorithm for graph coloring. It has been shown at least in some examples to perform somewhat better than other coloring heuristics in the context of Pauli string grouping [58] (a description of the method in this context can be found in the Supplemental Material of [55]). We can reduce the number of operators in the three-particle case from 25 to 12 using this method. The groups we have found are presented as an example in Appendix A. A comparison of the number of operators in the Pauli decomposition can be seen in Table I. By grouping some of the operators together, the number of operators needed for the measurement of the witness significantly decreases. Due to the grouping of operators, the cost for conducting the three-qubit experiment in the parallel setup seems relatively cheap; it reduces the number of operators that need to be measured to witness the entanglement from 25 to 12. The linear and star setups will not be considered in the remainder of this paper since they do not provide a better entanglement generation (see Fig. 2) or a better witness (see

<sup>&</sup>lt;sup>5</sup>By nonlocal operations we mean operations that act on several qubits and which cannot be applied to each qubit separately; these include, for instance, entangling operations or SWAP operations [57,58], which might be difficult to implement in practice.

TABLE I. Number of Pauli operators that make up the decomposed PPT witness and the number of Pauli operator groups for the different setups. Operator groups are formed by operators which can be measured together and can be found using the largest-degree-first coloring algorithm. The partial transpose is taken such that the witness is optimal. For the three-qubit case the second system is partial transposed as in Eq. (9)

$\overline{n}$	Setup	No. of operators	No. of operator groups
2	parallel	4	3
2	linear	9	8
3	parallel	26	12
3	linear	47	22
3	star	56	26

Fig. 3) and require more operator groups or operators to construct the witness (see Table I). The number of measurements needed to characterize entanglement by measuring the witness increases as the decoherence is introduced into the setup.

## V. DECOHERENCE

We have assumed so far that the system is completely unaffected by its environment. Given our aim is to estimate which setup is more appropriate, it is necessary to simulate a realistic case where we must consider the effects of decoherence. The interaction of the system with its environment causes the system to share, and subsequently potentially lose, this information information. This is defined as decoherence (see [45] for an introduction to decoherence theory). Although the decoherence is determined by the specific interactions with the environment, we can still consider a general approach. Assuming that the environmental state  $|E_i\rangle$  couples to the system's position states  $|\vec{x}(i)\rangle$  [66], we rewrite Eq. (1) to describe both the environment and the system:

$$|\Psi_0\rangle = \frac{1}{2^{3/2}} \sum_{j_1, j_2, j_3 = 0, 1} |\vec{x}(j_1)\vec{x}(j_2)\vec{x}(j_3)\rangle |E_{j_1}E_{j_2}E_{j_3}\rangle. \quad (12)$$

We have assumed that the qubits are independent of each other at t=0 s and that their coupling to the environment is independent [17]. The density matrix describing the environment and the system is found from Eq. (12) as usual:  $\rho(0) = |\Psi_0\rangle\langle\Psi_0|$ . We can extract the system's (s) entanglement by tracing out the environmental (e) degrees of freedom  $\rho_s = \text{Tr}_e(\rho) = \sum_i \langle E_i | \rho | E_i \rangle$ . We find

$$\rho_{S}(0) = \frac{1}{8} \sum_{j_{1}, j_{2}, j_{3} = 0, 1} |j_{1} j_{2} j_{3}\rangle \langle j_{1} j_{2} j_{3}| 
+ \frac{1}{8} \sum_{\substack{j_{1}, j_{2}, j_{3} = 0, 1 \\ j'_{1}, j'_{2}, j'_{3} = 0, 1}} |j_{1} j_{2} j_{3}\rangle \langle j'_{1} j'_{2} j'_{3}| \langle E_{j_{1}} E_{j_{2}} E_{j_{3}}| 
\times |E_{j'_{1}} E_{j'_{2}} E_{j'_{3}}\rangle.$$
(13)

Equation (13) shows that the system loses coherence as  $\langle E_{j_1,j_2,j_3}||E_{j'_1,j'_2,j'_3}\rangle \rightarrow 0$ . As is done in many decoherence models [66], we assume that the overlap between the environmental states decreases exponentially over time with a rate  $\gamma$ , known

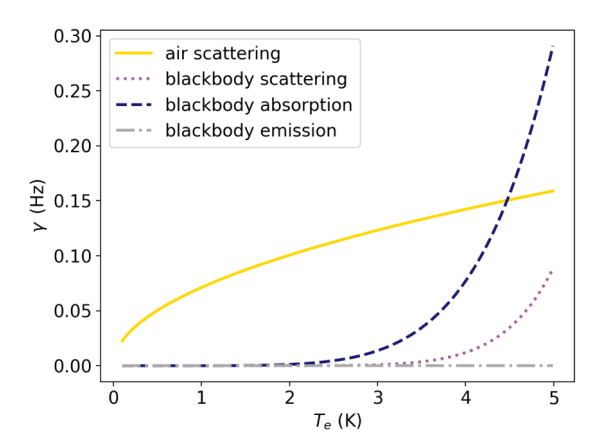


FIG. 4. Estimate of the decoherence rate due to interaction with air molecules and blackbody photons. For environmental temperatures  $T_e = 0.1$ –5 K the wavelength of the air molecules is much smaller (1–15 nm) and the wavelength of the blackbody photons is much larger (3–98 mm) than the superposition width (250  $\mu$ m). Therefore, we can use both the short- and long-wavelength limits to study their decoherence effects for this range of temperatures. The number density for the gas is taken to be  $N/V = 10^8$  m<sup>-3</sup>, the radius of the superposition particles is  $a = 10^{-6}$  m, and we have used the dielectric constant of a material similar to that of a diamond. From the figure we expect the decoherence rate of at least 0.5 Hz for the ambient temperatures  $T_e > 0.5$  K. The decoherence due to the blackbody emission is dependent on the internal temperature ( $T_i = 0.15$  K) and therefore has a constant value of  $\sim 10^{-10}$  Hz. See Appendix B for more details.

as the decoherence rate,

$$\langle E_j(t)||E_{j'}(t)\rangle \propto e^{-\gamma t}, \quad j \neq j'.$$

Clearly at t = 0 the states have not lost coherence. By time evolving Eq. (13), we obtain

$$\rho_{S}(\tau) = \frac{1}{8} \sum_{\substack{j_{1}, j_{2}, j_{3} = 0, 1 \\ j_{1}, j_{2}, j_{3} = 0, 1 \\ j'_{1}, j'_{2}, j'_{3} = 0, 1}} |j_{1}j_{2}j_{3}\rangle\langle j_{1}j_{2}j_{3}| 
+ \frac{1}{8} \sum_{\substack{j_{1}, j_{2}, j_{3} = 0, 1 \\ j'_{1}, j'_{2}, j'_{3} = 0, 1}} e^{-\delta\gamma\tau} e^{i(\phi_{j_{1}j_{2}j_{3}} - \phi_{j'_{1}j'_{2}j'_{3}})\tau} |j_{1}j_{2}j_{3}\rangle\langle j'_{1}j'_{2}j'_{3}|, \tag{14}$$

with  $\phi_{j_1j_2j_3}$  as given in Eq. (3) and  $\delta = 3 - \delta_{j_1j_1'} - \delta_{j_2j_2'} - \delta_{j_3j_3'} \in [1, 2, 3]$ . The exponential decay term causes the off-diagonal terms to go to zero over time, making it impossible to measure the entanglement and progressively transforming the experimental quantum state into a maximally mixed state. The presence of the environment provides a constraint on the experiment time  $\tau$ .

In Appendix B the interaction with the environment is studied in a more detailed fashion based on the analysis performed in [17]. The results of the calculations performed in this Appendix are represented in Fig. 4, which shows the estimated decoherence rate as a function of the ambient temperature. We estimate that  $\gamma > 0.05$  Hz for an environmental temperature of at least 0.5 K.

We have compared the witness expectation value for different decoherence rates  $\gamma$  in Fig. 5. However, due to the witness

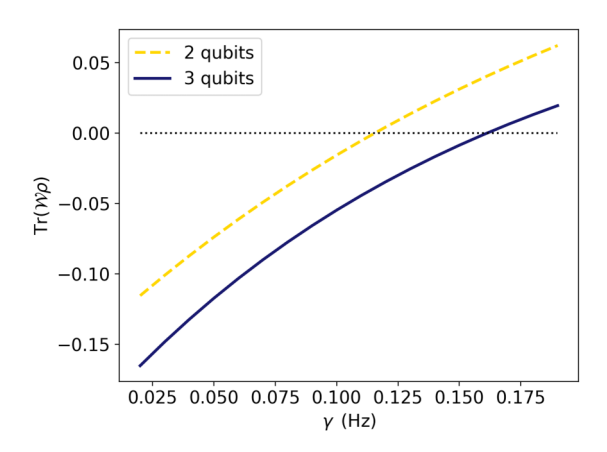


FIG. 5. The PPT entanglement witness expectation value is plotted for the two- and three-qubit parallel setups, for  $\gamma \in [0.02, 0.20]$  Hz and at  $\tau = 2.5$  s. The partial transpose for the three-qubit setup is taken over the second subsystem. The three-qubit setup is negative for higher decoherence rates compared to the two-qubit setup. In Appendix C we show that taking the partial transpose over the first subsystem does not give such an improvement in the witness. The dotted line indicates  $\text{Tr}(W\rho) = 0$ .

being basis dependent, this comparison should be considered with caution. The three-qubit parallel setup (where we take  $\rho^{T_2}$ ) seems to be robust against decoherence compared to the two-qubit setup. The PPT entanglement witness becomes positive at  $\tau=2.5$  s around  $\gamma>0.12$  Hz for n=2 and around  $\gamma>0.16$  Hz for n=3. In Fig. 16. in Appendix C we show that finding the witness by partially transposing the first qubit  $(\rho^{T_1})$  does not improve the witness compared to the two-qubit setup.

Figures 6 and 7 show the entanglement witness as a function of time for  $\gamma = 0.1$  Hz and  $\gamma = 0.15$  Hz, respectively. We see that the experiment time  $\tau$  is important in protecting the system against decoherence. Comparing the shapes of the lines in these figures also indicates that the three-qubit setup

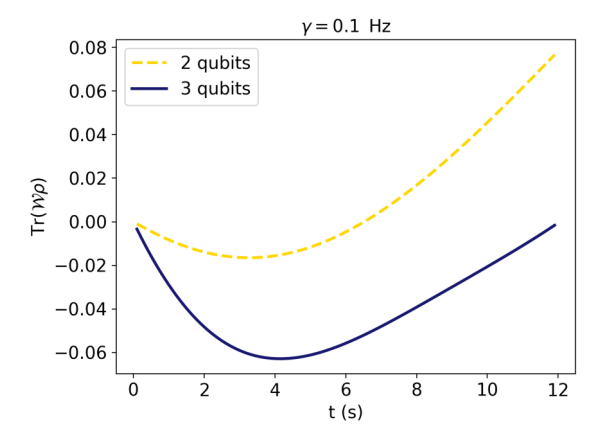


FIG. 6. The PPT entanglement witness expectation value over time for  $\gamma=0.1$  Hz for two and three qubits in the parallel setup. The partial transpose for the three-qubit setup is taken over the second subsystem. Due to the competition between the entanglement and the decoherence, the graphs will become positive at some point when the decoherence effects become too strong. This will happen sooner for the two-qubit setup than for the three-qubit setup.

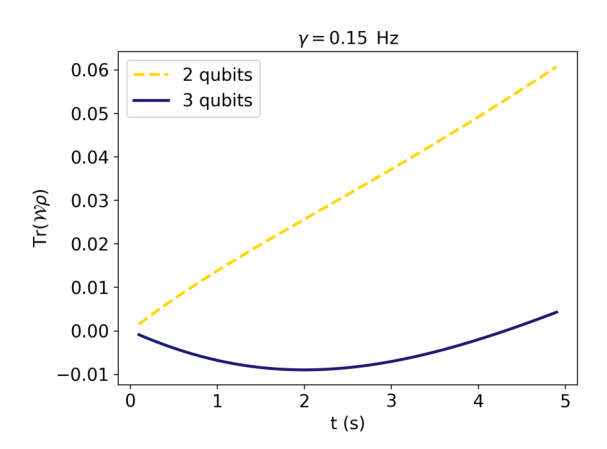


FIG. 7. The PPT entanglement witness expectation value over time for  $\gamma=0.15$  Hz for two and three qubits in the parallel setup. The partial transpose for the three-qubit setup is taken over the second subsystem. The witness for the two-qubit setup is never negative due to the strong decoherence effects. It is negative for about 4 s for the three-qubit setup.

will likely be more robust against decoherence since it has a steeper decrease. From Fig. 6 we can see that if the experiment takes a sufficiently long time, the entanglement will not be measurable for any of the systems considered as the witness will become positive due to the decoherence effects. In Fig. 7 the entanglement is seen to be undetectable for the two-qubit setup and only detectable for the three-qubit setup if  $\tau < 4 \text{ s}$ . The shapes of the curves in these two graphs are due to the competition between the entanglement and the decoherence.

Intuitively, the three-qubit setup is understood to be more robust against decoherence effects because of this competition between the entanglement of the subsystems and the decoherence. Since the three-qubit setup generates more entanglement between the subsystems within 5 s than the two-qubit setup (see Fig. 2), it takes more decoherence (meaning either a longer time or a higher decoherence rate) to destroy this entanglement between the subsystems. However, the fact that our three-qubit system is more robust against decoherence is not a general argument since the entanglement generation depends not only on the number of particles but also on the setup and the choice of subsystem, as discussed in Sec. II.

Our three-qubit setup looks very promising, but before drawing any conclusions we must simulate the number of measurements needed to witness the entanglement in a laboratory.

## VI. SIMULATING QGEM EXPERIMENT

The experimental simulations (by which we mean numerical simulation of the experiment statistics) are done in the same way as in Ref. [24]. The expectation value and the standard error are computed by repeatedly measuring the quantum state resulting from the experiment against the Pauli operators. For each fixed number of repeated measurements the confidence level of confirming that the state is entangled is found. A confidence interval  $\mathcal C$  for the expectation value of a witness  $\mathcal W$  can be computed as [24,67]

$$C_{\mathcal{W}} = [\langle \mathcal{W} \rangle - t_{\alpha} s_{\mathcal{W}}, \langle \mathcal{W} \rangle + t_{\alpha} s_{\mathcal{W}}], \tag{15}$$

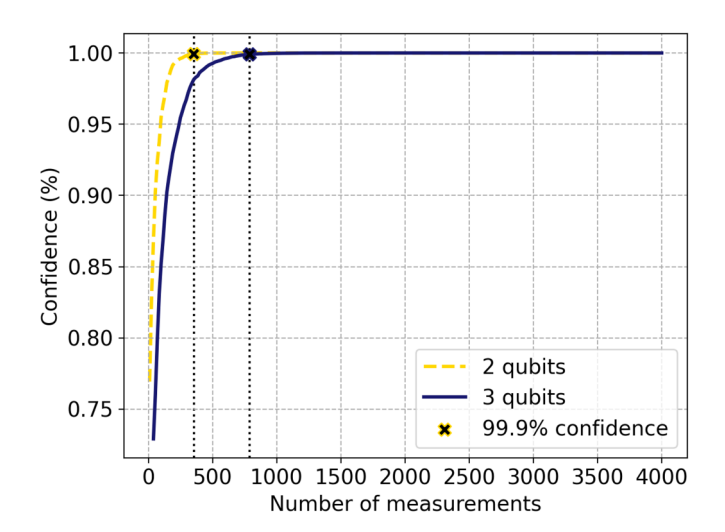


FIG. 8. Experimental simulation of the QGEM experiment for the two-qubit and three-qubit parallel setups at  $\tau=2.5$  s. The crosses indicate 99.9% confidence that the state is entangled. The witness expectation values are -0.146 for the two-qubit setup and -0.202 for the three-qubit setup (these can also be read off from Fig. 5).

with  $t_{\alpha}$  the *t*-value corresponding to the desired level of confidence and  $s_{\mathcal{W}}$  the standard error of the measurement population.<sup>6</sup> To estimate a given confidence level tested against the null hypothesis  $\langle \mathcal{W} \rangle \geqslant \mu_0$ , with  $\mu_0 = 0$ , we compute the *t*-values by performing a one-sided *t*-test<sup>7</sup> [24,67]

$$t = \frac{|\langle \mathcal{W} \rangle - \mu_0|}{s_{\mathcal{W}}}.$$
 (16)

The t-value provides us information about the probability of the expectation value  $\mathcal{W}$  being below the  $\mu_0$  (i.e., that we can reject the null hypothesis). To translate this information into a confidence level, we can look at a t-distribution table and recover the so-called p-value, which corresponds to the probability of making an error when rejecting the null hypothesis. Therefore, p is the probability that the true value of  $\mathcal{W}$  is above  $\mu_0 = 0$  despite the data gathered. To get the confidence level, we just need to compute 1 - p. (For further details refer to [67]; for another application to quantum observables refer to the Appendix of [24].) As discussed in Sec. IV, if the system is not confirmed to be entangled, it only means that the entanglement is not measurable. It does not necessarily mean that the system is separable.

Figure 8 compares the confidence levels given in Eq. (15) as a function of the number of measurements for the two- and

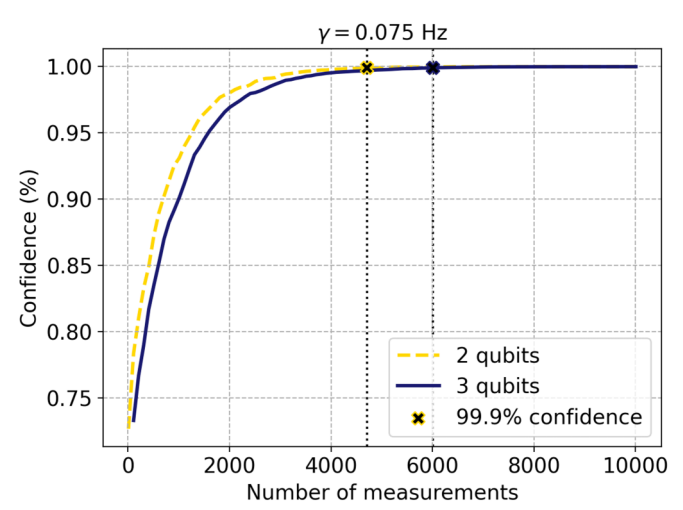


FIG. 9. Experimental simulation of the QGEM experiment for the two-qubit and three-qubit parallel setups with  $\gamma=0.075~{\rm Hz}$  and at  $\tau=2.5~{\rm s}$ . The crosses indicate 99.9% confidence for the entanglement; this number increases due to the introduction of the decoherence into the model. The witness expectation values are -0.043 for the two-qubit setups and -0.084 for the three-qubit setup (see Fig. 5).

three-qubit parallel setups after  $\tau=2.5$  s. Without the decoherence, due to the extra qubit in the three-qubit setup, more measurements are needed to confirm with confidence (99.9%) that the system is entangled. However, from the discussion in the preceding section we expect that if the decoherence is included, at some point while increasing the decoherence rate, the three-qubit setup will require fewer measurements due to it being more resistant to the effects of decoherence. Figure 9 compares the confidence levels given in Eq. (15) with a decoherence rate of  $\gamma=0.075$  Hz. Due to the introduction of the decoherence, the number of measurements needed to confirm the entanglement increases.

In Fig. 10 the confidence levels for the three-qubit parallel setup are shown for different decoherence rates  $\gamma \in [0.025\text{--}0.1]$  Hz. Comparing this to the two-qubit setup plotted in Fig. 11, we see that the number of measurements needed to confirm the entanglement with 99.9% confidence is lower for the two-qubit setup than for the three-qubit setup for the decoherence rates 0.025--0.075 Hz, although the difference is not very large. At higher decoherence rates ( $\gamma \geq 0.1$  Hz) the three-qubit setup needs fewer measurements compared to the two-qubit setup.

From Fig. 5 we can predict that the two-qubit setup has a negative witness at  $\tau = 2.5$  s for approximately  $\gamma < 0.12$  Hz. For 0.12 Hz  $< \gamma < 0.15$  Hz, we have to look at the three-qubit setup for measurements. The confidence level as a function of the number of measurements for the higher decoherence rates is plotted in Fig. 12.

Around  $\gamma > 0.15$  Hz, the three-qubit setup will probably start experiencing too much decoherence for it to detect any entanglement; this can already be seen from the  $\gamma = 0.15$  Hz graph in Fig. 12. The above results are summarized in Table II.

As discussed before in Sec. IV, the number of measurements can be reduced by grouping the operators that need to be measured. Table I showed the number of Pauli operator

<sup>&</sup>lt;sup>6</sup>The *t*-value is a measure of the difference between the data ( $\langle W \rangle$  in our case) and the null hypothesis ( $\mu_0 = 0$  in our case). In general, a larger *t*-value means that there is more evidence against the null hypothesis. For details about statistical testing and analysis we recommend [67]

 $<sup>^{7}</sup>$ A one-sided *t*-test, as opposed to a two-sided test, only performs statistical tests in one direction (instead of two). Since we are interested in rejecting the null hypothesis  $\langle \mathcal{W} \rangle \geqslant 0$ , a one-sided test is applicable.

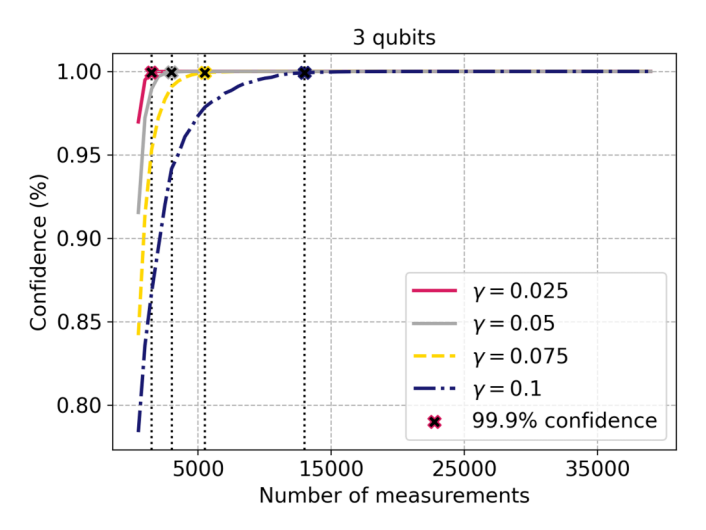


FIG. 10. Experimental simulation of the QGEM experiment for the three-qubit parallel setup for different decoherence rates at  $\tau=2.5$  s, with  $\gamma=[0.025, 0.050, 0.075, 0.1]$  Hz having the witness expectation values -0.156, -0.117, -0.084, and -0.055, respectively (see Fig. 5). The number of measurements needed to confirm the entanglement with the confidence increases for higher decoherence rates, but not as much as for the two-qubit setup.

groups for different witnesses; an example of the grouping is given in Appendix A. By measuring a group of operators simultaneously, the total number of measurements can drop considerably, as illustrated in Fig. 12 for decoherence rates  $\gamma=0.125$  and 0.15 Hz. The results from the experimental simulation with grouped operators are summarized in Table III. Performing measurements yields a marked improvement, especially for the three-qubit QGEM setup where the number of measurements at lower decoherence rates  $\gamma<0.6$  Hz become less than or approximately equal to the number

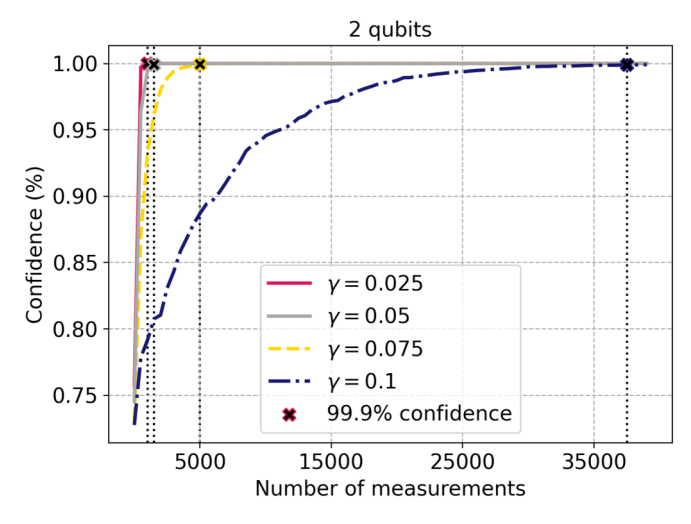


FIG. 11. Experimental simulation of the QGEM experiment for the two-qubit parallel setup for different decoherence rates at  $\tau = 2.5$  s, with  $\gamma = [0.025, 0.050, 0.075, 0.1]$  Hz having the witness expectation values -0.108, -0.074, -0.043, and -0.016, respectively (see Fig. 5). The number of measurements needed to confirm the entanglement increases for higher decoherence rates.

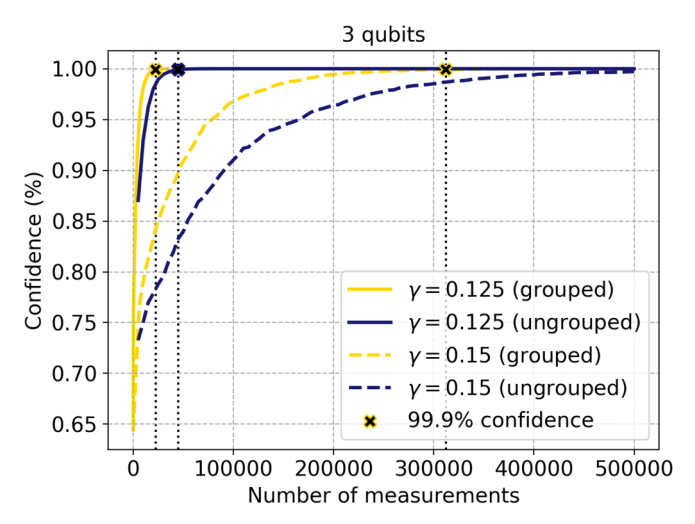


FIG. 12. Experimental simulation of the QGEM experiment for the three-qubit parallel setup at  $\tau=2.5$  s. For  $\gamma=0.125, 0.15$  Hz the witness expectation values are -0.030 and -0.008, respectively. The two-qubit setup cannot detect entanglement for these decoherence rates. Measurements with grouped operators reduce the number of measurements needed to confirm the entanglement.

TABLE II. Comparison of the approximate number of measurements needed to confirm the entanglement with 99.9% confidence for the n=2 and n=3 parallel setups under different decoherence rates at  $\tau=2.5$  s. The witness expectations values for n=2 for  $\gamma=[0.025, 0.050, 0.075, 0.1]$  Hz are -0.108, -0.074, -0.043, and -0.016, respectively; for  $\gamma>0.1$  Hz the witness becomes positive. The witness expectation values for n=3 for  $\gamma=[0.025, 0.050, 0.075, 0.1, 0.125, 0.15]$  Hz are -0.156, -0.117, -0.084, -0.055, -0.030, and -0.008, respectively.

γ (Hz)	n = 2	n = 3
0.025	~1000	~1500
0.05	$\sim$ 1500	~3000
0.075	$\sim$ 5000	~5500
0.1	$\sim \! \! 37500$	~13 000
0.125		~42 500
0.15		$\sim 750000$

TABLE III. Comparison of the approximate number of measurements needed to confirm entanglement with 99.9% confidence for the n=2 and n=3 parallel setups under different decoherence rates at  $\tau=2.5$  s. The number of measurements needed is reduced by doing the experimental simulation with the grouped operators (see Table I), as was discussed in Sec. IV.

γ (Hz)	n = 2	n = 3
0.025	~580	~640
0.05	~1250	~1390
0.075	~3900	~2900
0.1	$\sim$ 29 200	~6500
0.125		$\sim$ 22 400
0.15		~312 000

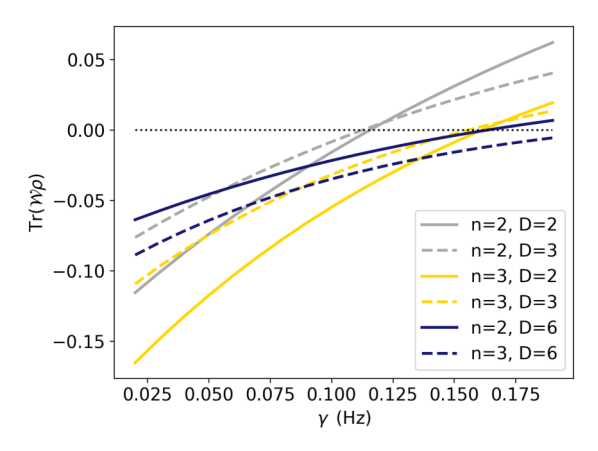


FIG. 13. The PPT entanglement witness is plotted for different setups at  $\tau=2.5$  s. Here n is the number of particles and D is the number of superposition states. All setups are parallel setups [Fig. 1(a)]. The dotted line indicates  $\text{Tr}(W\rho)=0$ . Adding a single qubit (increasing n by one) makes the setup more resilient against the decoherence compared to adding a single superposition state (increasing D by one). Taking n=2 and D=6 seems to have the same effect as adding a third qubit (n=3 and D=2). The n=3 and D=6 setup seems most resilient against decoherence, although for this setup the number of needed measurements will be extremely high.

of measurements needed for the two-qubit setup. This makes the three-qubit QGEM setup even more favorable.

# VII. QUBITS VS QUDITS

In Ref. [24] qudits (a superposition of D states<sup>8</sup>) instead of qubits (which are qudits with D=2) were proposed as a way to protect against the decoherence. Due to the increase in the number of measurements needed to confirm entanglement for qudit setups, that work concluded that qudits should be used only if the decoherence is sufficiently high such that the witness for the qubit setup becomes positive ( $\gamma > 0.12$  Hz). In Sec. VI we saw that the three-qubit setup also outperforms the two-qubit setup only for sufficiently high decoherence rates; therefore, we compare the two-qudit and three-qubit cases.

In Fig. 13 we compare the entanglement witness expectation value for n=2 and n=3 qubits (D=2) and qutrits (superposition of three states, D=3). There seems to be very little difference when switching from qubits to qutrits. It seems that switching from qubits to six-dimensional qudits has the same effect with respect to resilience against the decoherence as switching from the two-qubit to the three-qubit setup. However, the number of operators needed to measure the witness increases much more for the six-dimensional qudit case (94 operator groups) compared to the three-qubit case (12 operator groups). Table IV shows the number of operator (groups) in the witness for the setups considered in Fig. 13. From the two-qubit case, adding either one superposition dimension or one qubit does not differ much in the number of

TABLE IV. Number of Pauli operators that make up the decomposed PPT witness, the number of Pauli operator groups for the different number of qudits n, and different number of superposition states D.

n	D	No. of operators	No. of operator groups
2	2	4	3
3	2	26	12
2	3	77	14
2	6	1272	94

operator groups that are added (14 and 12 operator groups, respectively), but from Fig. 13 we infer that the three-qubit setup outperforms the two-qutrit setup.

For a better comparison, we look at the (grouped) measurement plots in Figs. 10 and 12 and compare them with the results from [24]. The number of measurements needed to reach a 99.9% confidence level in the entanglement is much higher for the six-dimensional two-qudit (n = 2 and D = 6)setup compared to the three-qubit setup: For  $\gamma = 0.125$  Hz, the six-dimensional two-qudit setup needs about 2000000 measurements (or 200 000 when grouping operators<sup>9</sup>), while the three-qubit setup needs about 42 500 measurements (or 22 400 when grouping operators). Reference [24] concluded that only for  $\gamma > 0.12$  Hz, it is favorable to use qudits over qubits, specifically the six-dimensional qudit setup. However, we find here that the three-qubit setup is even more favorable for these decoherence rates. One could also think about switching to three-qudit setups for improvement, which we will leave for future investigation. Looking at the results in [24], this would only be necessary for  $\gamma > 0.16$  Hz (when the three-qubit setup never has a negative witness). It might also be favorable to add a qubit instead of switching to qudits, but this is beyond the scope of the present paper.

## VIII. CONCLUSION

For the three-qubit case we studied three different setups: the parallel, the linear, and the star setup (see Fig. 1). We have found that the three-qubit parallel setup is optimal; it leads to the highest rate of the entanglement generation (Fig. 2) and in our chosen basis provides the best witness (Fig. 3). The chosen subsystem matters when analyzing the entanglement generation. Taking the partial trace or partial transpose of the second system is the most favorable since it has a shorter average distance to the other subsystems and therefore the highest interaction and the best generation of the entanglement.

Sections IV and V indicated that the three-qubit setup compared to the two-qubit setup provides a better witness (i.e., a more negative witness), which is also more resilient to the decoherence (i.e., the witness stays negative for a longer time and at higher decoherence rates). However, the cost of having a better witness by introducing an extra qubit is that

<sup>&</sup>lt;sup>8</sup>Experimentally, the number of superpositions states D can be seen as the number of arms in each interferometer. The number of particles n is the number of interferometers.

<sup>&</sup>lt;sup>9</sup>These numbers were derived in [24], where a different grouping strategy was used. It is worth noting that that grouping strategy may not be realizable in the actual experimental setting due to nonlocal operations.

it requires more measurements. In Sec. V we saw that the number of Pauli operators or operator groups in the witness increases for the three-qubit case. This was reflected in the number of measurements needed (see Sec. VI). Tables II and III showed that for smaller decoherence rates the two-qubit setup is favorable in terms of the number of measurements, while for higher decoherence rates the three-qubit setup is favorable. The turning point seems to be around  $\gamma=0.08$  Hz, or  $\gamma=0.06$  Hz when considering grouping the operators.

In Appendix B the decoherence rate was estimated. It was found that the decoherence rate is expected to be at least  $\gamma=0.05$  Hz for environmental temperatures of  $T\geqslant 0.5$  K (see Fig. 14). This is very close to the decoherence rate  $\gamma=0.06$  Hz, for which the three-qubit setup becomes favorable with respect to the number of measurements needed to confirm the entanglement up to 99.9% confidence level. Based on the estimation of the decoherence rate, the three-qubit QGEM protocol provides an improvement in the number of needed measurements compared to the original QGEM protocol. However, this is very much dependent on the expected decoherence rate and therefore on the experimental setting. The decoherence rate increases as the temperature of the environment increases; also it is highly dependent on the size of the superposition particles.

To give a better understanding of how realizable the threequbit QGEM protocol is in terms of number of measurements, we converted the number of measurements to experiment time. The interaction time was taken to be  $\tau = 2.5$  s and the time it takes to construct the superpositions and to bring the superpositions back together was taken to be 0.5 s [10]. For the smallest expected decoherence rate  $\gamma = 0.05$  Hz, 1390 measurements were needed to confirm entanglement with 99.9% confidence in the three-qubit parallel setup. The total experiment time would therefore be approximately (2.5 s +  $2 \times 0.5 \text{ s}) \times 1390 = 4865 \text{ s}$  (a similar time was found in the two-qubit case). The experiment would take about 1 h and 20 min excluding all the setup that needs to be done between consecutive measurements; this is realizable. For comparison, at  $\gamma = 0.1$  Hz the two-qubit system measurements would take 28.4 h, while the three-qubit system measurements take 6.3 h.

Additionally, the three-qubit system was compared to the two-qudit setups (Sec. VII). The two-qudit setup (n=2 and D=6) was found to be equally resilient against the decoherence as the three-qubit setup, but it requires far more measurements. The gain from switching to qudits is negated by the increase in the number of needed measurements, while

for a three-qubit system the number of measurements stays more feasible. For  $\gamma>0.16$  Hz the three-qubit setup cannot witness entanglement anymore, and one could consider switching to a three-qudit setup. However, since adding a qubit to the setup causes a clear improvement in the rate of entanglement generation, this begs the question of whether a four-, five-, or six-qubit setup could provide further improvements (specifically for  $\gamma>0.16$  Hz). We find that indeed increasing the number of qubits increases the system's resilience against the decoherence further. However, the extra qubits also require more operator groups to be measured and the key is to find a balance between these two to find the optimal experimental system.

## **ACKNOWLEDGMENTS**

M.S. was supported by the Fundamentals of the Universe research program within the University of Groningen. J.T. was supported by an industrial CASE studentship, funded by UK EPSRC (Grant No. EP/R513143/1), in collaboration with University College London and Rahko Ltd. R.J.M. was supported by a University College London departmental studentship. The research of A.M. was funded by the Netherlands Organisation for Science and Research Grant No. 680-91-119. S.B. would like to acknowledge EPSRC Grants No. EP/N031105/1 and No. EP/S000267/1.

## APPENDIX A: WITNESSING ENTANGLEMENT

For the two-qubit parallel setup the witness is given by [19]

$$W = \frac{1}{4}(1 - X \otimes X - Y \otimes Z - Z \otimes Y). \tag{A1}$$

In this case, the witness is composed of four operators. The identity term will always have an expectation value of 1 and therefore does not need to be measured. The three operators left, however, still needed to be measured separately when considering the grouping rules mentioned in the main text. Indeed, the first Pauli operators in each of the three tensor operators do not commute with one another, therefore failing the condition of qubitwise commutativity. There are means to still measure these operators together as they generally commute; however, this would require nonlocal operations [24], which we consider not so realistic in an experiment.

For the three-qubit parallel setup the witness for the middle qubit is

$$\mathcal{W} = \frac{1}{26} (1 - 1 \otimes 1 \otimes X - 1 \otimes X \otimes X - 1 \otimes Y \otimes Y - 1 \otimes Y \otimes Z - 1 \otimes Z \otimes Y - X \otimes 1 \otimes 1 - X \otimes X \otimes X - 1 \otimes X \otimes X - X \otimes Y \otimes Z - X \otimes Z \otimes Y - X \otimes Z \otimes Z - Y \otimes 1 \otimes Y - Y \otimes 1 \otimes Z - Y \otimes X \otimes Y - Y \otimes X \otimes Z - Y \otimes Y \otimes 1 - Y \otimes Z \otimes X - Z \otimes X \otimes X - Z \otimes 1 \otimes Y - Z \otimes X \otimes Y - Z \otimes X \otimes Z - Z \otimes Y \otimes 1 - Z \otimes Y \otimes X - Z \otimes Z \otimes X ).$$
 (A2)

Here we can indeed group the list of 26 operators (25 when discarding the identity term) into groups that commute qubitwise. As the first example of the rule, consider the first two operators (after the identity)  $1 \otimes 1 \otimes X$  and  $1 \otimes X \otimes X$ . Each

operator in the tensor commutes with the operator of the same index in the other tensor; they (qubitwise) commute and both can clearly be measured at the same time (if one collects measurements for  $1 \otimes X \otimes X$ , they can use the measurements on

the last operator to infer the expectation value of  $1 \otimes 1 \otimes X$ ). Based on this, we can group all 25 terms above into 12 groups, presented in Table V.

## APPENDIX B: ESTIMATING THE DECOHERENCE RATE

In [17] an explicit expression for  $\gamma$  was derived for the two-qubit QGEM setup. Therein decoherence due to the scattering between the environmental particles and the superpositions was considered. Since the environmental state (the state of the scattered particle) is dependent on the position of the test particle, the scattered particle shares information about the superposition state. For a large number of scatterings (so for a large scattering rate and/or after a long time) the system will decohere. We will use the result from Ref. [17] for the three-qubit setup discussed in this paper. The three superpositions are assumed to be spatially unaffected by scattering with the environment and independent of each other.

Following [17,45], we write the final state of the scattered particle that scattered off the system's position state  $|\vec{x}\rangle$  as

$$|E(\vec{x})\rangle = e^{-i\vec{q}\,\vec{x}/\hbar} \hat{S}_0 e^{i\vec{q}\,\vec{x}/\hbar} |E_i\rangle.$$
 (B1)

Here  $\vec{q}$  is the momentum of the scattered environmental particle and  $S_0$  is the scattering operator acting on the scattering center. The density-matrix element of the superposition with the scattered particle(s) traced out is given as

$$\rho_{S}(\vec{x}, \vec{x}') = |\vec{x}\rangle\langle \vec{x}'|\langle E(\vec{x})||E(\vec{x}')\rangle. \tag{B2}$$

This equation is similar to Eq. (13). It is clear that the diagonal terms  $\vec{x} = \vec{x}'$  are not affected by the environment. The expression for  $\langle E(\vec{x})||E(\vec{x}')\rangle$  was evaluated in the S-matrix formalism in [66].

We will consider the decoherence due to the scattering of the air molecules with the superposition, and scattering with and absorption and emission of the blackbody photons. These are thought to be the leading causes of decoherence for a macroscopic spatial superposition [17,66,68]. For these decoherence sources, we can simplify the decoherence rate because for the environmental temperature considered here they have either a much longer or shorter wavelength compared to the superposition width  $\Delta x$ .

TABLE V. Example of qubitwise commuting groups constructed using the operators composing the entanglement witness of the three-qubit setup (A2).

Group	Operators	
$1 \ 1 \otimes 1 \otimes X$	$1 \otimes X \otimes X  X \otimes 1 \otimes 1  X \otimes X \otimes 1$	$X \otimes X \otimes X$
2	$1 \otimes Y \otimes Y  Y \otimes 1 \otimes Y  Y \otimes Y \otimes 1$	
3	$1 \otimes Y \otimes Z  X \otimes Y \otimes Z$	
4	$1 \otimes Z \otimes Y  X \otimes Z \otimes Y$	
5	$Y \otimes 1 \otimes Z  Y \otimes X \otimes Z$	
6	$Y \otimes Z \otimes 1  Y \otimes Z \otimes X$	
7	$Z \otimes 1 \otimes Y  Z \otimes X \otimes Y$	
8	$Z \otimes 1 \otimes Z  Z \otimes X \otimes Z$	
9	$Z \otimes Y \otimes 1$ $Z \otimes Y \otimes X$	
10	$X\otimes Z\otimes Z$	
11	$Y \otimes X \otimes Y$	
12	$Z \otimes Z \otimes X$	

As discussed in Secs. II and III, we consider  $m \sim 10^{-14}$  kg and  $\Delta x = 250~\mu m$  for the setup. Furthermore, we take the internal temperature of the system to be  $T_i = 0.15$  K, the pressure of the environment to be  $10^{-15}$  Pa, and the test masses to be microcrystals (diamond) [10].

For an environmental temperature  $T_e \sim 0.15$  K, the wavelength of blackbody photons is  $\lambda_{bb} \sim 30$  mm [68]. This is much longer than the superposition width; therefore, the blackbody radiation can be evaluated in the long-wavelength limit. At the temperature  $T_e \sim 0.15$  K, the wavelength of the air molecules is  $\lambda_{air} \sim 0.82$  nm (with the mass of the scattering particle taken to be 28.97 u, which is the mass of a typical air molecule in the atomic mass units) [68]. This is much shorter than the superposition width, and the scattering with air molecules can therefore be evaluated in the shortwavelength limit.

For a constant superposition width, Refs. [17,45,66] found the decoherence rate due to short-wavelength and longwavelength particles to be

$$\gamma = \Gamma_{\rm air} + \Lambda_{\rm bb} \Delta x^2, \tag{B3}$$

where  $\Gamma_{\rm air}$  is the total scattering rate with the air molecules (short-wavelength limit contribution) and  $\Lambda_{\rm bb}$  is a scattering constant dependent on the density, velocity, and effective cross section for the blackbody radiation (long-wavelength limit contribution). The scattering rate  $\Gamma_{\rm air}$  depends also on the average velocity of the air molecules, the radius of the superposition qubit (taken to be of micron size with radius  $a=10^{-6}$  m), and the number density of the particles (taken to be  $N/V=10^8$  m<sup>-3</sup>, which corresponds to the vacuum pressure  $P=10^{-15}$  Pa). For our setup, we find

$$\Gamma_{\rm air} \sim 0.03 \; {\rm Hz}, \tag{B4}$$

where we used that  $\Gamma_{air} = \lambda_{air}^2 \Lambda_{air}$  [68] and that  $\Lambda_{air} \sim 4 \times 10^{16} \text{ s}^{-1} \text{ m}^{-2}$  for the pressure, test mass size, and temperature mentioned previously. We assumed that the environment is a perfect gas and used the formula provided in [45]:

$$\Lambda_{\text{air}} = \frac{8}{3\hbar^2} \frac{N}{V} a^2 \sqrt{2\pi m_{\text{air}}} (k_B T_e)^{3/2}.$$
 (B5)

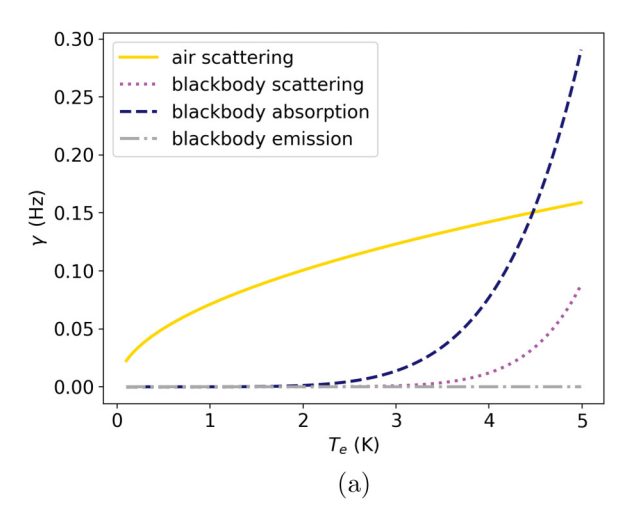
Now consider the scattering of the system with the blackbody photons. We find that

$$\Lambda_{\rm bb} \sim 0.003 \; {\rm s}^{-1} \, {\rm m}^{-2}$$
. (B6)

This consists of the blackbody scattering  $\Lambda_s$ , emission  $\Lambda_e$ , and absorption  $\Lambda_a$ ,  $\Lambda_{bb} = \Lambda_s + \Lambda_e + \Lambda_a$ . The scattering constants are determined by using the results found in [45], which models the scattering constant for the blackbody radiation and a particle modeled as the dielectric spheres with the radii a and the dielectric constant  $\epsilon$ . It is dependent also on Boltzmann's constant  $k_b$ , the reduced Planck constant  $\hbar$ , and the speed of light c:

$$\Lambda_s = 8! \frac{8}{9\pi} a^6 c \operatorname{Re} \left( \frac{\epsilon - 1}{\epsilon + 2} \right)^2 \left( \frac{k_b T_e}{\hbar c} \right)^9 \zeta(9).$$
 (B7)

The scattering constant depends heavily on the size of the test mass and the temperature of the environment. The



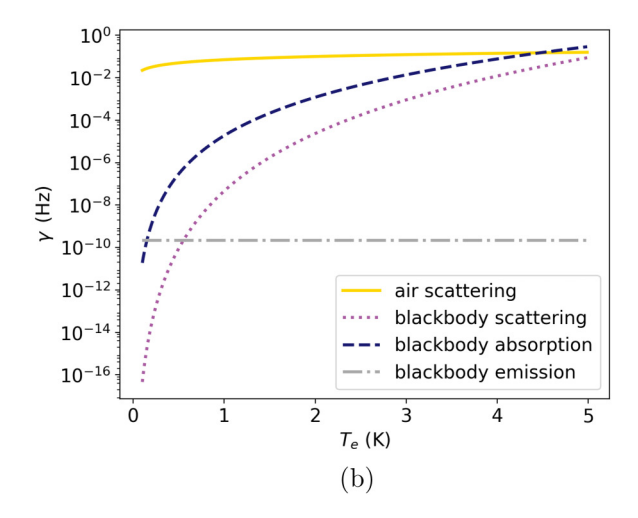


FIG. 14. Estimate of the decoherence rate due to interaction with the air molecules and the blackbody photons. For environmental temperatures  $T_e = 0.1$ –5 K the wavelength of the air molecules is much smaller (1–15 nm) and the wavelength of the blackbody photons is much larger (3–98 mm) than the superposition width (250  $\mu$ m). Therefore, we can use the short- and long-wavelength limits, respectively, to study their decoherence effects for this range of temperatures. For the decoherence rate due to the scattering off the air molecules, the number density for the gas is taken to be  $N/V = 10^8$  m<sup>-3</sup>. The radius of the particles is taken to be  $a = 10^{-6}$  m and we used the dielectric constant for diamond, with the internal temperature  $T_i = 0.15$  K. (a) This plot was used in Sec. V; it is based on the calculations performed in this Appendix. (b) Same data as in (a) but with a logarithmic scale on the y axis. From this figure we see clearly that the contribution to the decoherence rate from the blackbody emission is nonzero. It has a constant value of  $\sim 10^{-10}$  Hz since it is independent of the external temperature  $T_e$ .

constants were taken as described previously; furthermore,  $\zeta(n)$  is the Riemann  $\zeta$  function and the dielectric constant for diamond is  $\epsilon = 5.68 + 1.1 \times 10^{-4}i$ . This gives

$$\Lambda_s \sim 3 \times 10^{-8} \text{ s}^{-1} \text{ m}^{-2}.$$
 (B8)

The scattering constants  $\Lambda_e$  and  $\Lambda_a$  were determined in [17] by adjusting Eq. (B7) to use the probability of emission and absorption instead of the cross section of scattering. These are given by

$$\Lambda_{e(a)} = \frac{16\pi^5}{189} a^3 c \operatorname{Im}\left(\frac{\epsilon - 1}{\epsilon + 2}\right) \left(\frac{k_b T_{i(e)}}{\hbar c}\right)^6.$$
 (B9)

Note that for  $\Lambda_e$  we should use the temperature of the test mass ( $T_i = 0.15$  K), while for  $\Lambda_a$  we should use the temperature of the environment (also set to  $T_e = 0.15$  K). We find that

$$\Lambda_e = \Lambda_a \sim 0.003 \text{ s}^{-1} \text{ m}^{-2}.$$
 (B10)

Adding all the blackbody decoherence sources together, we get the value in Eq. (B6). Due to the blackbody photons, we thus have  $\Gamma_{bb} = \Lambda_{bb} \Delta x^2 \sim 4 \times 10^{-10}$  Hz.

For a higher environmental temperature of  $T_e = 1$  K, the approximations of the short- and long-wavelength limits still hold and we find

$$\begin{split} & \Lambda_e \sim 0.003 \; \text{s}^{-1} \, \text{m}^{-2}, \quad \Lambda_a \sim 0.3 \times 10^3 \; \text{s}^{-1} \, \text{m}^{-2}, \\ & \Lambda_s \sim 0.7 \; \text{s}^{-1} \, \text{m}^{-2}, \quad \Lambda_{air} \sim 7 \times 10^{17} \; \text{s}^{-1} \, \text{m}^{-2} \end{split}$$

so that  $\Gamma_{bb} \sim 10^{-5}$  Hz and  $\Gamma_{air} \sim 0.07$  Hz. The suspected decoherence rate is dependent on the temperature of the environment. In Fig. 14 the decoherence rate is plotted as a function of the environmental temperature.

Figure 14 depends greatly on the assumed experimental parameters. The expected decoherence rate decreases (increases) when the number density N/V, the size of the superposition a, and the external temperature  $T_e$  are decreased (increased). Changing the material (and thus the dielectric constant  $\epsilon$ ) also changes the expected decoherence rate, although it only influences the decoherence rate due to the blackbody photons, which for  $T \leq 3$  K is dominated by the decoherence due to the scattering with air molecules. As can be seen from Eqs. (B5), (B7), and (B9), the decoherence rate is highly sensitive to the size of the test particle and the temperature of the environment.

So far we have considered decoherence sources during the part of the experiment where the qubits are interacting for a time  $\tau_{\rm int}$ . Additionally, decoherence plays a role while creating and bringing back together the superpositions. In this paper the decoherence during the creating and reuniting of the superpositions has not been taken into account. If we were to take this into account, we would also have to include the entanglement generation during these steps. The influence of the decoherence and the entanglement generation during creation and destruction of the superposition should be the subject of a separate paper.

## APPENDIX C: SUPPLEMENTARY ANALYSIS

In Fig. 2 the entanglement entropy was shown as a function of time for  $\tau \in [0, 5]$  s. For an extended period of time, we find the result given in Fig. 15. This time frame is of course not realistic for an experiment; however, in the reader's interest we wanted to illustrate the cyclical behavior of entanglement entropy.

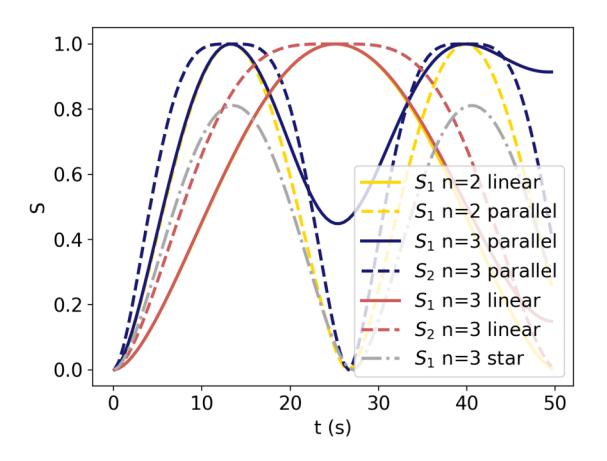


FIG. 15. Comparison of the entanglement entropy generated within  $\tau \in [0, 50]$  s. Note that, due to symmetry, for the parallel and linear setup we have  $S_1 = S_3$  and for the star setup we have  $S_1 = S_2 = S_3$ . The lines representing  $S_1$ , n = 3 linear and  $S_1$ , n = 2 linear setups almost overlap. During the first 10 s the rate of entanglement generated by the  $S_2$ , n = 3 parallel setup is highest; however, this timescale is unrealistic experimentally.

Figure 16 is supplemental to the analysis performed in Sec. III, which showed that taking the partial trace over the outer systems provided the highest rate of entanglement generation. From Fig. 2 we saw that the rate of entanglement generation for the three-qubit system  $S_1$  compared to the two-qubit system almost overlaps, while the rate of entanglement generation for the three-qubit system  $S_2$  is clearly higher.

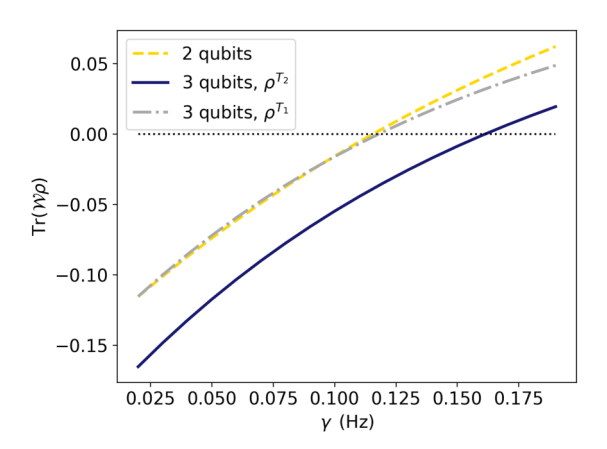


FIG. 16. The PPT entanglement witness expectation value is plotted for the two- and three-qubit parallel setups for  $\gamma \in [0.02, 0.20]$  Hz and at  $\tau = 2.5$  s. The partial transpose for the three-qubit setup can be taken over the second subsystem (denoted by  $\rho^{T_2}$ ) or over the first subsystem (denoted by  $\rho^{T_1}$ , which, due to the symmetry of the setup, is the same as  $\rho^{T_3}$ ). The partition  $\rho^{T_2}$  is negative for higher decoherence rates compared to the two-qubit setup and  $\rho^{T_1}$ . Taking the partial transpose over the first subsystem does not give an improvement in the witness. The dotted line indicates  $\text{Tr}(\mathcal{W}\rho) = 0$ .

Figure 16 shows the same but in terms of the witness. The witness expectation value of the three-qubit setup with the partial transpose of the first subsystem  $\rho^{T_1}$  almost overlaps with the witness expectation value for the two-qubit setup. Taking the partial transpose of the middle subsystem  $\rho^{T_2}$  provides a witness that is more resistant against decoherence.

- [1] C. Kiefer, *Quantum Gravity* (Oxford University Press, Oxford, 2014), pp. 709–722.
- [2] S. N. Gupta, Gravitation and electromagnetism, Phys. Rev. 96, 1683 (1954).
- [3] R. P. Feynman, Quantum theory of gravitation, Acta Phys. Pol. **24**, 697 (1963).
- [4] B. S. DeWitt, Quantum theory of gravity. I. The canonical theory, Phys. Rev. **160**, 1113 (1967).
- [5] B. S. DeWitt, Quantum theory of gravity. II. The manifestly covariant theory, Phys. Rev. **162**, 1195 (1967).
- [6] F. Dyson, Is a graviton detectable? in *Proceedings of the XVI-Ith International Congress on Mathematical Physics, Aalborg, 2012*, edited by A. Jensen (World Scientific, Singapore, 2014), pp. 670–682.
- [7] G. Baym and T. Ozawa, Two-slit diffraction with highly charged particles: Niels Bohr's consistency argument that the electromagnetic field must be quantized, Proc. Natl. Acad. Sci. U.S.A. 106, 3035 (2009).
- [8] A. Ashoorioon, P. S. Bhupal Dev, and A. Mazumdar, Implications of purely classical gravity for inflationary tensor modes, Mod. Phys. Lett. A 29, 1450163 (2014).
- [9] J. Martin and V. Vennin, Obstructions to Bell CMB experiments, Phys. Rev. D 96, 063501 (2017).
- [10] S. Bose, A. Mazumdar, G. W. Morley, H. Ulbricht, M. Toroš, M. Paternostro, A. A. Geraci, P. F. Barker, M. S. Kim, and

- G. Milburn, Spin Entanglement Witness for Quantum Gravity, Phys. Rev. Lett. **119**, 240401 (2017).
- [11] R. J. Marshman, A. Mazumdar, and S. Bose, Locality and entanglement in table-top testing of the quantum nature of linearized gravity, Phys. Rev. A 101, 052110 (2020).
- [12] C. Marletto and V. Vedral, Gravitationally Induced Entanglement Between Two Massive Particles is Sufficient Evidence of Quantum Effects in Gravity, Phys. Rev. Lett. 119, 240402 (2017).
- [13] A. Belenchia, R. M. Wald, F. Giacomini, E. Castro-Ruiz, I. C. V. Brukner, and M. Aspelmeyer, Quantum superposition of massive objects and the quantization of gravity, Phys. Rev. D 98, 126009 (2018).
- [14] H. C. Nguyen and F. Bernards, Entanglement dynamics of two mesoscopic objects with gravitational interaction, Eur. Phys. J. D 74, 69 (2020).
- [15] J. S. Pedernales, G. W. Morley, and M. B. Plenio, Motional Dynamical Decoupling for Interferometry with Macroscopic Particles, Phys. Rev. Lett. 125, 023602 (2020).
- [16] R. J. Marshman, A. Mazumdar, R. Folman, and S. Bose, Large splitting massive Schrödinger kittens, arXiv:2105.01094.
- [17] T. W. van de Kamp, R. J. Marshman, S. Bose, and A. Mazumdar, Quantum gravity witness via entanglement of masses: Casimir screening, Phys. Rev. A 102, 062807 (2020).

- [18] M. Toroš, A. Mazumdar, and S. Bose, Loss of coherence of matter-wave interferometer from fluctuating graviton bath, arXiv:2008.08609.
- [19] H. Chevalier, A. J. Paige, and M. S. Kim, Witnessing the nonclassical nature of gravity in the presence of unknown interactions, Phys. Rev. A 102, 022428 (2020).
- [20] M. Toroš, T. W. van de Kamp, R. J. Marshman, M. S. Kim, A. Mazumdar, and S. Bose, Relative acceleration noise mitigation for nanocrystal matter-wave interferometry: Applications to entangling masses via quantum gravity, Phys. Rev. Research 3, 023178 (2021).
- [21] M. Christodoulou and C. Rovelli, On the possibility of laboratory evidence for quantum superposition of geometries, Phys. Lett. B **792**, 64 (2019).
- [22] M. Christodoulou and C. Rovelli, On the possibility of experimental detection of the discreteness of time, Front. Phys. 8, 207 (2020).
- [23] Y. Margalit, O. Dobkowski, Z. Zhou, O. Amit, Y. Japha, S. Moukouri, D. Rohrlich, A. Mazumdar, S. Bose, C. Henkel, and R. Folman, Realization of a complete Stern-Gerlach interferometer: Toward a test of quantum gravity, Sci. Adv. 7, eabg2879 (2021).
- [24] J. Tilly, R. J. Marshman, A. Mazumdar, and S. Bose, Qudits for witnessing quantum gravity induced entanglement of masses under decoherence, Phys. Rev. A 104, 052416 (2021).
- [25] D. Carney, H. Müller, and J. M. Taylor, Using an atom interferometer to infer gravitational entanglement generation, PRX Quantum 2, 030330 (2021).
- [26] R. Howl, V. Vedral, D. Naik, M. Christodoulou, C. Rovelli, and A. Iyer, Non-Gaussianity as a signature of a quantum theory of gravity, PRX Quantum 2, 010325 (2021).
- [27] D. Miki, A. Matsumura, and K. Yamamoto, Entanglement and decoherence of massive particles due to gravity, Phys. Rev. D 103, 126017 (2021).
- [28] A. Matsumura and K. Yamamoto, Gravity-induced entanglement in optomechanical systems, Phys. Rev. D 102, 106021 (2020).
- [29] S. Qvarfort, S. Bose, and A. Serafini, Mesoscopic entanglement through central–potential interactions, J. Phys. B 53, 235501 (2020).
- [30] H. Miao, D. Martynov, H. Yang, and A. Datta, Quantum correlations of light mediated by gravity, Phys. Rev. A 101, 063804 (2020).
- [31] T. Weiss, M. Roda-Llordes, E. Torrontegui, M. Aspelmeyer, and O. Romero-Isart, Large Quantum Delocalization of a Levitated Nanoparticle using Optimal Control: Applications for Force Sensing and Entangling via Weak Forces, Phys. Rev. Lett. 127, 023601 (2021).
- [32] A. Datta and H. Miao, Signatures of the quantum nature of gravity in the differential motion of two masses, Quantum Sci. Technol. 6, 045014 (2021).
- [33] T. Krisnanda, G. Y. Tham, M. Paternostro, and T. Paterek, Observable quantum entanglement due to gravity, npj Quantum Inf. 6, 12 (2020).
- [34] S. A. Haine, Searching for signatures of quantum gravity in quantum gases, New J. Phys. 23, 033020 (2021).
- [35] E. Schrödinger, Discussion of probability relations between separated systems, Proc. Cambridge Philos. Soc. **31**, 555 (1935).

- [36] C. H. Bennett, D. P. DiVincenzo, J. A. Smolin, and W. K. Wootters, Mixed-state entanglement and quantum error correction, Phys. Rev. A 54, 3824 (1996).
- [37] R. Horodecki, P. Horodecki, M. Horodecki, and K. Horodecki, Quantum entanglement, Rev. Mod. Phys. 81, 865 (2009).
- [38] P. van Nieuwenhuizen, On ghost-free tensor Lagrangians and linearized gravitation, Nucl. Phys. B 60, 478 (1973).
- [39] T. Biswas, T. Koivisto, and A. Mazumdar, Nonlocal theories of gravity: The flat space propagator, arXiv:1302.0532.
- [40] S. Rijavec, M. Carlesso, A. Bassi, V. Vedral, and C. Marletto, Decoherence effects in non-classicality tests of gravity, New J. Phys. 23, 043040 (2021).
- [41] B. Yi, U. Sinha, D. Home, A. Mazumdar, and S. Bose, Massive spatial qubits for testing macroscopic nonclassicality and Casimir induced entanglement, arXiv:2106.11906.
- [42] T. Biswas, A. Mazumdar, and W. Siegel, Bouncing universes in string-inspired gravity, J. Cosmol. Astropart. Phys. 03 (2006) 009.
- [43] T. Biswas, E. Gerwick, T. Koivisto, and A. Mazumdar, Towards Singularity and Ghost Free Theories of Gravity, Phys. Rev. Lett. 108, 031101 (2012).
- [44] S. Bose, A. Mazumdar, M. Schut, and M. Toroš, Mechanism for the quantum natured gravitons to entangle masses, arXiv:2201.03583.
- [45] M. A. Schlosshauer, *Decoherence and the Quantum-to-Classical Transition* (Springer Science + Business Media, New York, 2007).
- [46] J. von Neumann, *Mathematical Foundations of Quantum Mechanics* (Princeton University Press, Princeton, 2018).
- [47] M. A. Nielsen and I. L. Chuang, *Quantum Computation and Quantum Information* (Cambridge University Press, Cambridge, 2002).
- [48] P. Hyllus, O. Gühne, D. Bruß, and M. Lewenstein, Relations between entanglement witnesses and bell inequalities, Phys. Rev. A **72**, 012321 (2005).
- [49] M. Horodecki, P. Horodecki, and R. Horodecki, Separability of *n*-particle mixed states: Necessary and sufficient conditions in terms of linear maps, Phys. Lett. A **283**, 1 (2001).
- [50] A. Peres, Separability Criterion for Density Matrices, Phys. Rev. Lett. 77, 1413 (1996).
- [51] O. Gühne and G. Tóth, Entanglement detection, Phys. Rep. 474, 1 (2009).
- [52] K.-C. Ha and S.-H. Kye, Construction of three-qubit genuine entanglement with bipartite positive partial transposes, Phys. Rev. A 93, 032315 (2016).
- [53] D. J. Griffiths, Introduction to Quantum Mechanics (Prentice Hall, Upper Saddle River, 1995).
- [54] T.-C. Yen, V. Verteletskyi, and A. F. Izmaylov, Measuring all compatible operators in one series of single-qubit measurements using unitary transformations, J. Chem. Theory Comput. 16, 2400 (2020).
- [55] I. Hamamura and T. Imamichi, Efficient evaluation of quantum observables using entangled measurements, npj Quantum Inf. 6, 56 (2020).
- [56] P. Gokhale O. Angiuli, Y. Ding, K. Gui, T. Tomesh, M. Suchara, M. Martonosi, and F. T. Chong, O(N³) measurement cost for variational quantum eigensolver on molecular Hamiltonians, IEEE Trans. Quantum Eng. 1, 1 (2020).
- [57] P. Gokhale, O. Angiuli, Y. Ding, K. Gui, T. Tomesh, M. Suchara, M. Martonosi, and F. T. Chong, Minimizing state

- preparations in variational quantum eigensolver by partitioning into commuting families, arXiv:1907.13623.
- [58] O. Crawford, B. van Straaten, D. Wang, T. Parks, E. Campbell, and S. Brierley, Efficient quantum measurement of Pauli operators in the presence of finite sampling error, Quantum 5, 385 (2021).
- [59] A. Peruzzo, J. McClean, P. Shadbolt, M.-H. Yung, X.-Q. Zhou, P. J. Love, A. Aspuru-Guzik, and J. L. O'Brien, A variational eigenvalue solver on a photonic quantum processor, Nat. Commun. 5, 4213 (2014).
- [60] J. R. McClean, J. Romero, R. Babbush, and A. Aspuru-Guzik, The theory of variational hybrid quantum-classical algorithms, New J. Phys. 18, 023023 (2016).
- [61] A. Kandala, A. Mezzacapo, K. Temme, M. Takita, M. Brink, J. M. Chow, and J. M. Gambetta, Hardware-efficient variational quantum eigensolver for small molecules and quantum magnets, Nature (London) 549, 242 (2017).
- [62] C. Hempel, C. Maier, J. Romero, J. McClean, T. Monz, H. Shen, P. Jurcevic, B. P. Lanyon, P. Love, R. Babbush, A.

- Aspuru-Guzik, R. Blatt, and C. F. Roos, Quantum Chemistry Calculations on a Trapped-Ion Quantum Simulator, Phys. Rev. X 8, 031022 (2018).
- [63] N. C. Rubin, R. Babbush, and J. McClean, Application of fermionic marginal constraints to hybrid quantum algorithms, New J. Phys. 20, 053020 (2018).
- [64] C. Kokail, C. Maier, R. van Bijnen, T. Brydges, M. K. Joshi, P. Jurcevic, C. A. Muschik, P. Silvi, R. Blatt, C. F. Roos, and P. Zoller, Self-verifying variational quantum simulation of lattice models, Nature (London) 569, 355 (2019).
- [65] D. J. A. Welsh and M. B. Powell, An upper bound for the chromatic number of a graph and its application to timetabling problems, Comput. J. 10, 85 (1967).
- [66] M. Schlosshauer, The quantum-to-classical transition and decoherence, arXiv:1404.2635.
- [67] M. Dekking, A Modern Introduction to Probability and Statistics: Understanding Why and How (Springer, London, 2005).
- [68] O. Romero-Isart, Quantum superposition of massive objects and collapse models, Phys. Rev. A 84, 052121 (2011).